An Augmented Catenary Model for Underwater Tethered Robots

Martin Filliung, Juliette Drupt, Charly Peraud, Claire Dune, Nicolas Boizot, Andrew Comport, Cedric Anthierens, Vincent Hugel

An Augmented Catenary Model for Underwater Tethered Robots

M. Filliung[1, 2], J. Drupt[1], C. Peraud[1], C. Dune[1], N. Boizot[2], A. Comport[3], C. Anthierens[1], V. Hugel[1]

***Abstract*— This paper examines the relevance of using catenary-based curves to model cables in underwater tethered robotic applications in order to take into account the influence of hydrodynamic damping. To this end, an augmented catenary-based model is introduced to deal with the dynamical effects of surge motion, sway motion or a combination of both on a cable. Experimental studies are carried out with eight cables of varying stiffness, weight and buoyancy. One end of the cable is fixed, while the other end is moved by the underwater robot. The obtained results help to determine which cables and which dynamics are compatible with a fair estimation of the cable shape through the proposed models.**

I. Introduction

Remotely Operated Vehicles (ROVs) are used to explore unknown areas. Their tether is the only way to provide direct feedback to the pilot, as electromagnetic waves are absorbed in the first few centimetres of water. However, the tether can interfere with the robot's movement and, if its shape is not controlled, it can become entangled in obstacles. This is even more critical when exploring confined karstic terrain, wrecks or offshore installations with small observation ROVs. This study focuses on shape estimation of tethers of a few metres in length, *e.g.* the portion of cable connecting two mini-ROVs of a chain [1] or a mini-ROV to an Unmanned Surface Vehicle (USV) [2]. To be used in robot control for path following and obstacle avoidance, the chosen geometric model must be parametrised and fast to compute.

The standard catenary model, bound to a vertical plane, is defined as the shape of an idealized homogeneous hanging cable with fixed length and fixed ends, only subject to its own weight in the air. The catenary shape can be determined knowing the cable's length and its deflection. Depending on the available sensors, its shape can be estimated either from the relative position of the two attachment points such as in [3], [4] or from the local cable tangent orientation [5].

However, the extension of the catenary model to an underwater cable is not straightforward in the presence of hydrodynamic effects. In static conditions, submarine cables are only subject to weight and buoyancy. While the quasi-static assumption remains applicable for aerial cables at low speed when air friction can be neglected, the underwater drag involves hydrodynamic forces that move the cable from its vertical plane, even at low speed [6].

The main contribution of the present study is the introduction of a new enhanced catenary model that incorporates full tilting of the tether during surge or sway motion of the underwater robot. The relevance of this geometric model is confirmed by experiments conducted on eight cables with different mechanical properties (Fig. 1).

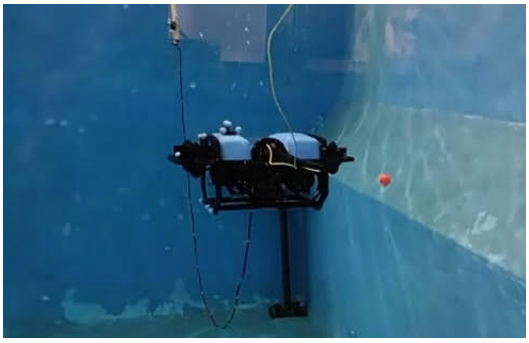

Fig. 1: Experimental setup. A dark red cable connects the ROV to a fixed point. Optical markers are regularly placed on the cable for underwater motion tracking. The slack light yellow tether is used for communications with the ROV.

The paper is organized as follows. Section II presents related work on underwater tethered robots and cable shape estimation. Section III introduces the augmented catenary model. The experimental protocol and data analysis are detailed in Section IV. Section V concludes the study and outlines future work.

II. Related work

Tethered robots are particularly common in underwater robotics, where cables are the only way to provide real time communication between ROVs and the surface [2]. Multiple underwater robots can also be connected together in order to communicate freely and share resources. In [7], small vehicles are connected to a bigger autonomous submarine. In addition, underwater robot chains are being investigated in order to limit the mechanical impact of tethers on ROV navigation and control by the addition of multiple mini-ROV on the cable to control its shape [1], [5]. It results in an additional underwater tethered robot configuration in which small devices are linked together by short cable portions.

The safe control of tethered robotic systems strongly relies on cable shape knowledge: on the one hand, controlling tethered robots requires knowledge of the cable's state [1], on the other hand, cable shape knowledge gives information about the localization of the robot at its end point [8], [9]. Some underwater cables are designed as proprioceptive sensors in order to measure their own shape. Optical-fiber cables measure their deformations using reflectometry techniques [10], [11]. Such cables can be used to locate

[1]COSMER Laboratory, Univ. de Toulon, France
[2]Univ. de Toulon, Aix Marseille Univ, CNRS LIS, Marseille, France
[3]CNRS I3S Laboratory, Univ. Côte d'Azur, Sophia Antipolis, France

Manuscript 633 submitted to 2024 IEEE International Conference on Robotics and Automation (ICRA). Received September 15, 2023.

connected underwater vessels [7]. Another version of optical fiber cable shape sensing consists in adding an external optical fiber sensor coating on a cable [12]. Such cables are, however, fragile and extremely expensive. The cable shape can also be estimated from the measurements of inertial sensors placed along it [13]. However, these methods require the use of a specially designed cable. In addition, the accuracy of these methods decreases with the cable's length due to error accumulation, e.g. approx. $1\,\mathrm{cm}$ error for a $1\,\mathrm{m}$ long optical fiber cable [10].

Other strategies make use of physical or geometrical cable models. A physical model can be developed based on the cable's hydrodynamics and the forces acting upon it [14], [15], [16], [17]. Although such models are the most comprehensive and designed to closely match the physics, they are computationally intensive and require an extensive understanding of multiple parameters which are difficult to measure under actual circumstances, such as water current or thruster parameters. As a result, simpler models are often preferred. The cable may be constrained to a simplified geometric shape artificially, for instance by introducing weights or sliding floaters to make it piecewise linear [18], [19], [9]. Some studies employ the catenary model, an hyperbolic curves, for underwater or aerial settings [1], [5], whereas parabolic curves may also be utilized in aerial scenarios [20].

However, in the presence of external forces, including ambient currents, hydrodynamic damping during motion, the geometric models that represent quasi-static cable shapes may not be accurate enough. A preliminary study [6] investigated the accuracy of an inclined catenary model for short cables connecting a pair of moving robots, using motion tracking of genuine cables. This paper expands on the findings of the study by presenting an enhanced parameterized model that considers complete cable inclination caused by external forces underwater.

III. Modeling and Estimation

Let $\mathcal{F}_w = (\mathbf{O}_w, \mathbf{x}_w, \mathbf{y}_w, \mathbf{z}_w)$ be a fixed Cartesian reference frame with the $\mathbf{z}_w$-axis vertical and pointing upwards.

A. Standard catenary model

The shape of a homogeneous hanging cable, with fixed length L, only subjected to its weight and buoyancy, is defined by a standard catenary curve (Fig. 2). The catenary lies in a vertical plane $\mathcal{P}_v = (\mathbf{O}_v, \mathbf{x}_v, \mathbf{z}_v)$, associated to the Cartesian frame $\mathcal{F}_v = (\mathbf{O}_v, \mathbf{x}_v, \mathbf{y}_v, \mathbf{z}_v)$ where $\mathbf{O}_v$ is the lowest point of the curve, $\mathbf{x}_v$ is horizontal and $\mathbf{z}_v$ is collinear to $\mathbf{z}_w$. Curve points coordinates $({}^vX, {}^vZ) \in \mathcal{P}_v$ are given by:

$$({}^vX, {}^vZ) \in [{}^vX_i, {}^vX_f] \times \mathbb{R} \text{ such that}$$
$${}^vZ = \frac{\cosh({}^vXC) - 1}{C} \tag{1}$$

where $C \in \mathbb{R}_+^*$ is the catenary parameter, and indexes i and f refer to the curve's endpoints. The left superscript indicates the frame in which a coordinate is given.

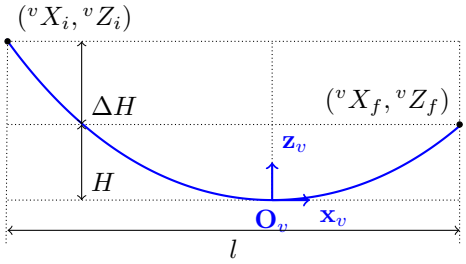

Fig. 2: Catenary curve of length L defined in $\mathcal{P}_v$. Parameters are the sag H, the difference of elevation ΔH and the horizontal distance l between attachment points.

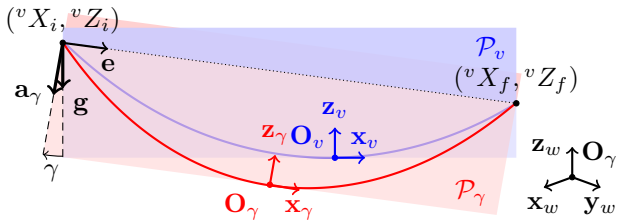

Fig. 3: Standard (blue) and γ-augmented (red) catenary for $\gamma = 10°$.

B. Augmented catenary model

As soon as the underwater cable is moved fast enough, hydrodynamics forces become non-negligible. The drag force dampens the movement with an amplitude that is proportional to the square of the speed. This effect is amplified by the added mass when significant accelerations are present [21], [14].

In the steady state case where all points on the cable move at the same velocity, they are subjected to the same drag forces. As a consequence, the resulting uniform acceleration of the cable is tilted, and its intensity is increased depending on the velocity. The addition of two degrees of freedom in the cable shape model to account for this effect is used here to extend the standard catenary model.

The first degree of freedom is a rotation of angle γ around the catenary axis $\mathbf{e}$, which is defined as the unit vector that connects cable endpoints [5] (Fig. 3). This is to consider the deformations of a tether subjected to sway motions, *i.e.* the cable ends move out of the vertical plane, namely $\mathcal{P}_v$. This rotation applied to $\mathcal{F}_v$ and $\mathcal{P}_v$ gives $\mathcal{F}_\gamma = (\mathbf{O}_\gamma, \mathbf{x}_\gamma, \mathbf{y}_\gamma, \mathbf{z}_\gamma)$ and $\mathcal{P}_\gamma$, respectively.

The second degree of freedom, a rotation of angle θ in $\mathcal{P}_\gamma$ (Fig. 4), considers tether deformations caused by surge motions, *i.e.* the two cable ends get closer or further away. The approximation of uniform hydrodynamic forces along the cable results in a uniform tilted acceleration $\mathbf{a}_{\theta\gamma}$ with respect to gravity. Let $\mathcal{F}_{\theta\gamma} = (O_{\theta\gamma}, \mathbf{x}_{\theta\gamma}, \mathbf{y}_{\theta\gamma}, \mathbf{z}_{\theta\gamma})$ be the associated Cartesian frame where $\mathbf{z}_{\theta\gamma}$ is parallel to $\mathbf{a}_{\theta\gamma}$ and $\mathbf{y}_{\theta\gamma}$ is parallel to $\mathbf{y}_\gamma$. The two ends of the cable can be expressed in $\mathcal{F}_{\theta\gamma}$ and (1) is used to construct the oriented catenary. This 2-DOF model is named the *$\theta\gamma$-augmented model*.

Note that zero values for γ and θ yield the *standard*

Manuscript 633 submitted to 2024 IEEE International Conference on Robotics and Automation (ICRA). Received September 15, 2023.

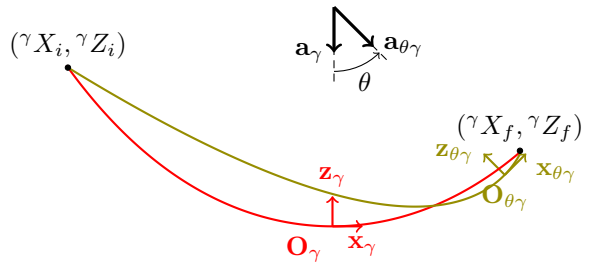

Fig. 4: γ-augmented (red) and $\theta\gamma$-augmented (green) catenary for $\theta = 45°$.

catenary model. If θ only is set to zero, the model presented in [5] can be obtained, and is referenced as γ-*augmented*.

C. Curvilinear discretization and residual

Let us consider $n+1$ 3D measurement points distributed along the cable's length. Accordingly, the model is discretized with respect to the curvilinear abscissa.

Henceforth, the symbols m, v, γ and $\theta\gamma$ are used as indexes referring to the measurements and the estimates of the *standard*, γ-augmented and $\theta\gamma$-augmented catenary model variations, respectively. Model points are written:

$$
\begin{gathered}
{}^{w}\mathbf{P}_k^* = ({}^{w}X_k^*, {}^{w}Y_k^*, {}^{w}Z_k^*) \\
k \in \{0, \dots, n\}, * \in \{m, v, \gamma, \theta\gamma\}
\end{gathered}
$$

where indexes $k = 0$ and $k = n$ are the tether endpoints, also indexed i and f.

Model variants accuracies are computed by means of the residuals:

$$
\varepsilon_{\mathbf{P}}^{*} = \frac{1}{n} \sum_{k=0}^{n} \| {}^{w}\mathbf{P}_k^m - {}^{w}\mathbf{P}_k^* \|, \ * \in \{v, \gamma, \theta\gamma\} \tag{2}
$$

D. Model parameters estimation

1) Catenary parameter: Let L be the known tether length, l the horizontal distance and ΔH the difference in elevation between the tether attachment points calculated from the measurements of the initial and final attachment points ${}^{\Diamond}\mathbf{P}_i^m$ and ${}^{\Diamond}\mathbf{P}_f^m$, with $\Diamond \in \{v, \gamma, \theta\gamma\}$ the frame in which the points are expressed (Fig. 2). The catenary parameter C is estimated by finding the root of function f which relates the curve's length and C [1] (using Brent's method [22]):

$$
f(C) = C^2 \left(L^2 - \Delta H^2\right) - 4 \sinh^2(lC/2)
$$

2) Augmented model parameters: Let $\varepsilon_{\mathbf{P}}^{\theta\gamma}(\theta, \gamma)$ be the accuracy written as a function of θ and γ (2). Angles θ and γ are estimated by minimizing this function by means of the trust region reflective algorithm [23]:

$$
(\theta, \gamma) = \underset{(\theta,\gamma)\in[-\pi,\pi]^2}{\operatorname{argmin}} \ \varepsilon_{\mathbf{P}}^{\theta\gamma}(\theta, \gamma)
$$

The initial estimates θ_0 and γ_0 are respectively set to zero and to the angle between $\mathcal{P}_{\gamma_0}$ and $\mathcal{P}_v$, where $\mathcal{P}_{\gamma_0}$ is the closest plane to all measured points.

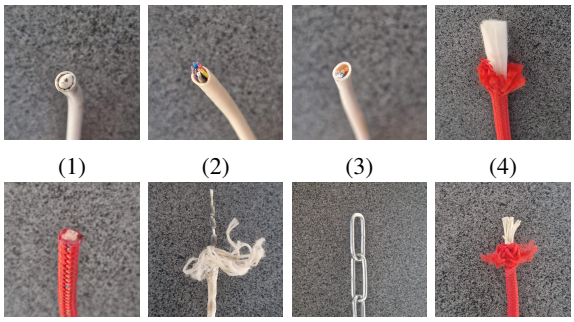

Fig. 5: Cables ends: (1) coaxial cable, (2) four-pair network cable, (3) two-pair network cable, (4) floating braided rope, (5) sail rope, (6) leaded seamstress rope, (7) plain steel chain, (8) elastic.

TABLE I: Cables characteristics

cable #	1	2	3	4
diameter / m	0.007	0.005	0.004	0.008
weight / N	1.079	0.687	0.392	0.294
buoyancy / N	0.049	0.147	−0.049	−0.491
wet weight / N	1.079	0.687	0.392	0.981
plastic deformation	✓	✓	✓	×
cable #	**5**	**6**	**7**	**8**
diameter / m	0.006	0.004	—	0.005
weight / N	1.079	1.373	3.120	0.589
buoyancy / N	0.245	1.177	2.708	0.098
wet weight / N	1.570	1.521	3.120	0.687
plastic deformation	×	×	×	×

IV. Experiments

A. Cables description

The experiments involve eight 3 m long cables presented in Fig. 5. These cables are meant to reflect the full range of mechanical characteristics found in robot umbilicals and tethers: stiffness from the most flexible to the most rigid; neutral, positive or negative buoyancy; elastic or nonelastic (Table I). Overall, these cables can be classified into two categories based on their capacity to retain plastic deformation: cables 1, 2 and 3 do, and cables 4, 5, 6, 7 and 8 do not. Cables 4, 6 and 7, are expected to give the best results in catenary shape fitting due to their clear positive or negative buoyancy, highlighted in Table I.

B. Experimental setup

The experiment is set up in a 7.2 m long, 4.2 m wide and 3 m deep tank. One end of the cable, namely ${}^{w}\mathbf{P}_n^m$, is attached to a ROV (BlueROV), while the other, namely ${}^{w}\mathbf{P}_0^m$, is fixed and attached to the side of the pool (Fig. 1).

The cable's and robot's positions are recorded by a 5-camera, 100 Hz *Qualisys*[1] underwater motion capture system. The robot as well as each cable are equipped with passive reflective markers and the cable's markers are evenly spaced out by 0.2 m ($n = 15$). The calibration of the motion capture

[1]See specifications at www.qualisys.com/cameras/underwater

Manuscript 633 submitted to 2024 IEEE International Conference on Robotics and Automation (ICRA). Received September 15, 2023.

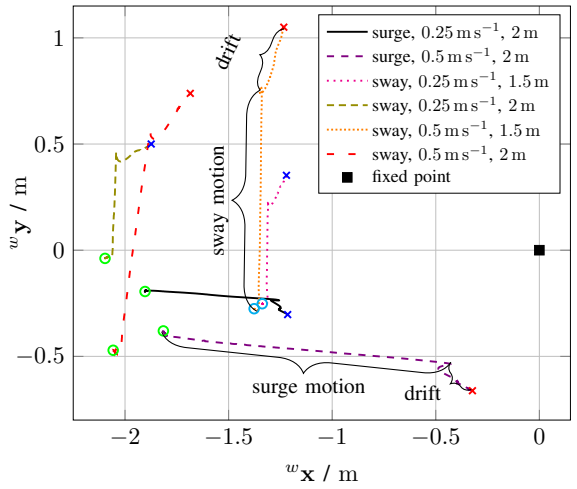

Fig. 6: Top view of typical trajectories of cable 6 end. Circles refer to initial positions and crosses refer to final positions.

system gives a standard deviation of $2.2\,\mathrm{mm}$ across the pool's volume for a known object's length. The points ${}^{w}\mathbf{P}_k^m$ are measured in the *Qualysis* world Cartesian frame which is defined by the positioning of a calibration target that may not be perfectly vertical in the real experiment. This introduces a small offset ($\pm 0.05\,\mathrm{rad}$) for the steady state angles as it can be seen in Fig. 8.

The initial position of the robot is defined such that the robot is stabilized at $1\,\mathrm{m}$ depth and approximately $1\,\mathrm{m}$ from the lateral pool wall facing the fixed attachment point (Fig. 6). Surge and sway movements are conducted individually to investigate the cable's response movement within or without its original vertical plane. The robot repeats the same open-loop control in sway or surge with the same step profile one after the other for each cable: 1) stabilisation with auto-depth at $1\,\mathrm{m}$ depth for $2\,\mathrm{s}$, 2) abrupt start with constant surge or sway command applied for $2.5\,\mathrm{s}$, 3) reversing of the thrusters for $0.3\,\mathrm{s}$ with a doubled velocity of opposite direction, to obtain an abrupt stop, 4) slow down the thruster for half the initial velocity during $0.2\,\mathrm{s}$ and 5) deactivation of the auto-depth control and complete stop of the thrusters after $13\,\mathrm{s}$. The robot then drifts slowly.

The starting position of the mini-ROV is manually determined with the help of a visual reference point. It is not always perfectly aligned with the fixed point (see starting circles and trajectories in Fig. 6). To address this problem, closed-loop control could be considered. However, conventional position sensors such as IMUs, DVLs and USBLs are not suitable for an experiment in a compact metal tank, and the use of a visual target limits the range of possible movements. Another option would be to use a traction bench. However, such a setup would not be representative of the dynamics of the mini-ROV in interaction with its tether. Nevertheless, the depth sensor allows for closed-loop depth control and the desired direction of motion was dominant with its open-loop controller.

The experiment is repeated three times for each cable, under six experimental conditions, which makes it possible to test the reactions of more or less taut cables with accelerations of different amplitudes. Each experimental condition is a combination of a direction of motion (sway or surge), a speed ($0.3\,\mathrm{m\,s^{-1}}$ or $0.6\,\mathrm{m\,s^{-1}}$) and a starting point characterized by its horizontal distance from the fixation point (about $1.5\,\mathrm{m}$ or $2\,\mathrm{m}$).

C. Results

1) General study: Figure 7 represents the residuals (2) for the three model variants, namely standard Catenary, γ-augmented and $\theta\gamma$-augmented, for all sequences and all experimental conditions. There is a general trend showing that the $\theta\gamma$-augmented model has lower residuals than the standard catenary model and the γ-augmented one. The γ-augmented variant is also more accurate than the standard catenary model.

Regardless of the experimental condition, cable 6 and 7 show lower residuals for all three variants, as expected regarding their physical properties (see Table I). Indeed, these cables are the closer to the definition of the catenary because they are flexible and negatively buoyant. Sail rope 5 and elastic rope 8 are also negatively buoyant but lighter with regards to their volume so their residual is higher. Indeed, the drag forces damping effects wins over the weight. The floating cable 4 behaves like an inverted catenary. It has a high residual for the standard catenary model (2^{nd} worst median) but shows a good fit for the $\theta\gamma$-augmented model (3^{rd} best median).

For the stiffer cables 1, 2 and 3, the improvement in accuracy for the $\theta\gamma$-augmented variant still exists, albeit to a lesser extent. Indeed, the stiffer the cable, the higher the residuals. These cables have permanent deformations as a result of being coiled. Furthermore they are neutrally buoyant. As a result, the impact of weight is insufficient to generate the catenary shape.

The section below examines the three model variants in greater details, distinguishing between the experiments involving predominant surge and sway motion. Cables 3, is chosen as representative of the stiff cables with neutral buoyancy and cable 6 is chosen among the flexible cables that are negatively buoyant (as defined in IV-A).

2) Detailed analysis of cables 3 and 6 as group representatives: Tables II and III show the box plots of the model residuals for cable 3 and 6 according to experimental parameters. First, the sway movements are displayed for a distance of $2\,\mathrm{m}$ and two different velocities. Then the sway movements are detailed for two different velocities and two starting points. These Tables show that the improvements of accuracy of the $\theta\gamma$-augmented model is consistent across experimental parameters.

For both groups representatives, the residuals of the models are smaller for slower movements and greater distance from the attachment point (*i.e.* more tension in the cable). The γ-augmented model displays a higher accuracy for lateral sway movements compared to forward surge movements. Conversely, our $\theta\gamma$-augmented is significantly better

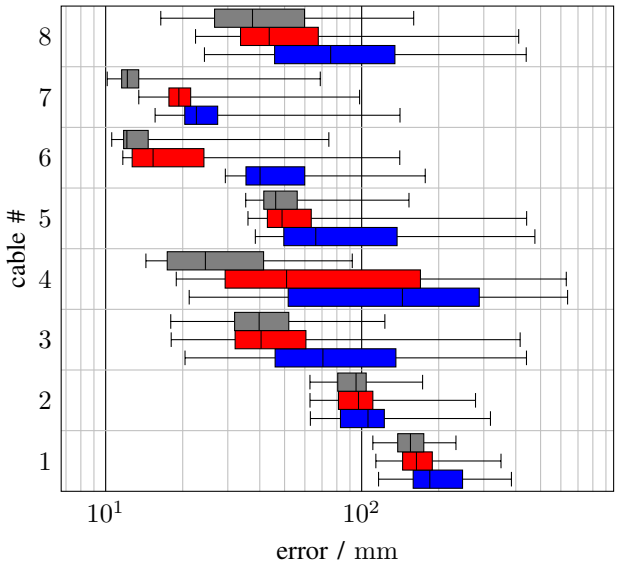

Fig. 7: Box plots of all 8 cables under all experimental parameters (speed, direction, distance) with the median, 1st and 3rd quartile, the 1st and 99th percentile of model residuals $\varepsilon^v_{\mathbf{P}}$ (blue), $\varepsilon^{\gamma}_{\mathbf{P}}$ (red) and $\varepsilon^{\theta\gamma}_{\mathbf{P}}$ (gray).

TABLE II: Box plots of the two-pair network cable, cable 3 residuals $\varepsilon^v_{\mathbf{P}}$ in blue, $\varepsilon^{\gamma}_{\mathbf{P}}$ in red and $\varepsilon^{\theta\gamma}_{\mathbf{P}}$ in gray

Experimental parameters	Box plot
surge, $0.3\,\mathrm{m\,s^{-1}}$, $2.0\,\mathrm{m}$	
surge, $0.6\,\mathrm{m\,s^{-1}}$, $2.0\,\mathrm{m}$	
sway, $0.3\,\mathrm{m\,s^{-1}}$, $1.5\,\mathrm{m}$	
sway, $0.3\,\mathrm{m\,s^{-1}}$, $2.0\,\mathrm{m}$	
sway, $0.6\,\mathrm{m\,s^{-1}}$, $1.5\,\mathrm{m}$	
sway, $0.6\,\mathrm{m\,s^{-1}}$, $2.0\,\mathrm{m}$	
error / mm	10^1 10^2

for surge movements in comparison of the γ-augmented. The gain in accuracy is even greater for cable 6's group.

3) Detailed analysis for experimental conditions of 0.6 m s^{-1} speed and 2 m distance for cables 3 and 6 as group representatives: Fig. 8 shows the three model variants residuals, angles θ and γ, as well as the robot's speed. These figures show in detail the different phases of the movement: an initial stable position (hydrostatic equilibrium phase), an abrupt start (dynamic phase), a phase of continuous application of a constant command (steady state phase), an abrupt stop (dynamic phase) and a subsequent hydrostatic phase.

A clear correlation appears between the robot's dynamics and the angle γ for sway motion. The estimated γ angle consistently increases with speed during sway movements,

TABLE III: Box plots of the leaded seamstress rope, cable 6 residuals $\varepsilon^v_{\mathbf{P}}$ in blue, $\varepsilon^{\gamma}_{\mathbf{P}}$ in red and $\varepsilon^{\theta\gamma}_{\mathbf{P}}$ in gray

Experimental parameters	Box plot
surge, $0.3\,\mathrm{m\,s^{-1}}$, $2.0\,\mathrm{m}$	
surge, $0.6\,\mathrm{m\,s^{-1}}$, $2.0\,\mathrm{m}$	
sway, $0.3\,\mathrm{m\,s^{-1}}$, $1.5\,\mathrm{m}$	
sway, $0.3\,\mathrm{m\,s^{-1}}$, $2.0\,\mathrm{m}$	
sway, $0.6\,\mathrm{m\,s^{-1}}$, $1.5\,\mathrm{m}$	
sway, $0.6\,\mathrm{m\,s^{-1}}$, $2.0\,\mathrm{m}$	
error / mm	10^1 10^2

whereas θ remains close to zero (Fig. 8a and 8b). As anticipated, surge movements have a noticeable impact on cable 3's estimated angle θ, with γ maintaining a small value (Fig. 8c). For cable 6, both angles increase with velocity, with θ being greater than the one observed for sway movement (Fig. 8d). However, since γ is larger than expected, let us examine the trajectory displayed in Fig. 6 relative to surge motion with $0.6\,\mathrm{m\,s^{-1}}$ and $2\,\mathrm{m}$. While the primary motion is surge, the trajectory of the robot is not precisely aligned with the fixed point causing the cable to move laterally. Although this effect is present throughout all sequences, it is particularly pronounced in this trajectory which explains the values for γ. This demonstrates that our $\theta\gamma$-augmented model is capable of simultaneously managing significant sway and surge movements. Finally, one can clearly see that cable 6 restores balance towards the vertical plane and the standard model at a faster rate compared to the lighter cable 3. As a result, physics-based modelling of angle dynamics opens up promising perspectives for model-based control synthesis.

V. Conclusion

This work introduced an augmented catenary model that accounts for the hydrodynamic effects on the tether when the ROV performs surge and sway motion. It incorporates the models presented in the state of the art, which can be found by zeroing one or both of the angles proposed as augmentation parameters.

The results drawn from the experiments carried out on eight different cables show that the augmented model provides a better estimate of the shape of all cables during dynamic phases, compared with the standard catenary model. The accuracy is best for flexible cables with adequate negative buoyancy. In addition, cables with the lowest residuals relative to the standard catenary model lead to the best improvements in accuracy using the augmented model. Their measured shape features greater planarity and homogenous tilting of their support plane during motion.

Manuscript 633 submitted to 2024 IEEE International Conference on Robotics and Automation (ICRA). Received September 15, 2023.

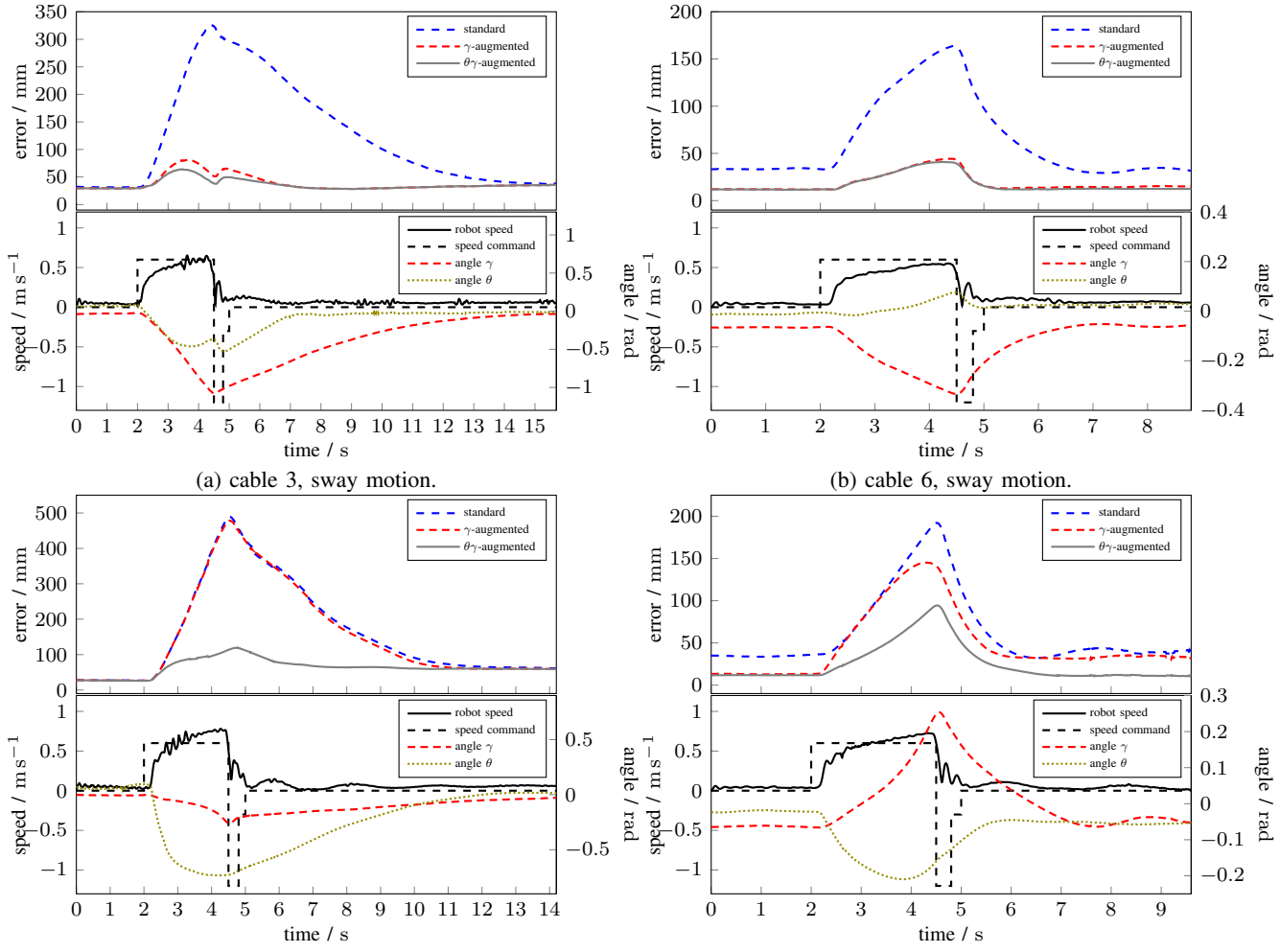

(a) cable 3, sway motion.

(b) cable 6, sway motion.

(c) cable 3, surge motion.

(d) cable 6, surge motion.

Fig. 8: Model residuals, robot speed and θ, γ angles over time. Speed command of $0.6\,\mathrm{m\,s^{-1}}$ and $2\,\mathrm{m}$ distance.

In light of these results, the augmented catenary model will be used in model-based controllers to estimate cable shape and its lowest position for deployment scenarios of tethered robots.

VI. Acknowledgment

This work is funded by the French Research Ministry, the CARTT de l'Université de Toulon.

References

[1] M. Laranjeira, C. Dune, and V. Hugel, "Catenary-based visual servoing for tether shape control between underwater vehicles," *Ocean Eng.*, vol. 200, p. 107018, 2020.

[2] O. Tortorici, C. Anthierens, V. Hugel, and H. Barthelemy, "Towards active self-management of umbilical linking rov and usv for safer submarine missions," in *IFAC-PapersOnline*, vol. 52, no. 21, Daejeon, Rep.of Korea, 2019, pp. 265–270.

[3] D. S. D'Antonio, G. A. Cardona, and D. Saldaña, "The catenary robot: Design and control of a cable propelled by two quadrotors," *IEEE Rob. and Autom. Lett.*, vol. 6, no. 2, pp. 3857–3863, 2021.

[4] D. S. D'Antonio and D. Saldana, "Folding knots using a team of aerial robots," in *IEEE/RSJ Int. Conf. on Intelligent Rob. and Sys.*, Oct. 2022.

[5] J. Drupt, C. Dune, A. I. Comport, S. Sellier, and V. Hugel, "Inertial-Measurement-Based Catenary Shape Estimation of Underwater Cables for Tethered Robots," in *IEEE/RSJ Int. Conf. on Intelligent Rob. and Sys.*, Kyoto, Japan, Oct. 2022.

[6] J. Drupt, C. Dune, A. I. Comport, and V. Hugel, "Validity of the catenary model for moving submarine cables with negative buoyancy," in *3rd IEEE IROS Workshop ROMADO-SI*, Kyoto, Japan, 2022.

[7] S.-C. Yu, J. Yuh, and J. Kim, "Armless underwater manipulation using a small deployable agent vehicle connected by a smart cable," *Ocean Eng.*, vol. 70, no. 23, pp. 149–159, 2013.

[8] P. McGarey, K. MacTavish, F. Pomerleau, and D. Barfoot, "Tslam: Tethered simultaneous localization and mapping for mobile robots," *Int. J. of Rob. Research*, vol. 36, no. 12, pp. 1363–1386, 2017.

[9] C. Viel, J. Drupt, C. Dune, and V. Hugel, "ROV localization based on umbilical angle measurement," *Ocean Eng.*, vol. 269, p. 113570, Feb. 2023.

[10] R. G. Duncan, M. E. Froggatt, S. T. Kreger, R. J. Seeley, D. K. Gifford, A. K. Sang, and M. S. Wolfe, "High-accuracy fiber-optic shape sensing," in *Sensor Sys and Networks*, K. J. Peters, Ed., vol. 6530, Int. Society for Optics and Photonics. San Diego, CA, USA: SPIE, 2007, pp. 487 – 497.

[11] I. Floris, J. M. Adam, P. A. Calderón, and S. Sales, "Fiber optic shape sensors: A comprehensive review," *Optics and Lasers in Eng.*, vol. 139, p. 106508, 2021.

[12] C. Xu, K. Wan, J. Chen, C. Yao, D. Yan, and C. Wang, "Underwater cable shape detection using shapetape," in *MTS/IEEE Oceans*, 2016, pp. 1–4.

[13] J. Frank, R. Geiger, D. R. Kraige, and A. Murali, "Smart tether system for underwater navigation and cable shape measurement," 2013, uS Patent 8,437,979.

[14] N. O.A. and I. Schjølberg, "Finite element cable-model for remotely operated vehicles (rovs) by application of beam theory," *Ocean Eng.*,

vol. 163, pp. 322–336, 2018.

[15] Y. Meng, X. Xu, and M. Zhao, "Dynamics calculation of complex deep-sea cable system based on hybrid optimization algorithm," *Ocean Eng.*, vol. 200, p. 107041, 2020.

[16] S. Soylu, B. Buckham, and R. Podhorodeski, "Dynamics and control of tethered underwater-manipulator systems," in *Oceans*. Seattle, WA, USA: MTS/IEEE, 2010, pp. 1–8.

[17] S. Hong, K. Ha, and J. Kim, "Dynamics modeling and motion simulation of usv/uuv with linked underwater cable," *J. of Marine Science and Engineering*, vol. 8, no. 5, 2020.

[18] C. Viel, "Self-management of the umbilical of a rov for underwater exploration," *Ocean Eng.*, vol. 248, p. 110695, Mar. 2022.

[19] ——, "Self-management of ROV umbilical using sliding buoys and stop," *IEEE Rob. and Autom. Lett.*, vol. 7, no. 3, pp. 8061–8068, July 2022.

[20] L. Smolentsev, A. Krupa, and F. Chaumette, "Shape visual servoing of a tether cable from parabolic features," in *IEEE Int. Conf on Rob. and Autom.*, London, United Kingdom, May 2023.

[21] T. Fossen, *Handbook of Marine Craft Hydrodynamics and Motion Control*, 05 2011.

[22] R. P. Brent, *Algorithms for minimization without derivatives*. Courier Corporation, 2013.

[23] M. A. Branch, T. F. Coleman, and Y. Li, "A subspace, interior, and conjugate gradient method for large-scale bound-constrained minimization problems," *SIAM Journal on Scientific Computing*, vol. 21, no. 1, pp. 1–23, 1999.